Nigerian Journal of Mathematics and Applications
Volume **36**, (2026), 47 − 62. *Printed by Unilorin press*
©*Nig. J. Math. Appl.*
http://www.njmaman.com

Two-Dimensional Laminar Boundary Layers Hydromagnetic Arrhenius Kinetics Dissipative Fluid Reactive Flow in Non-Slip Conditions with Variable Properties

R. A. Kareem[1*], L. A. Animashaun[2] and J. O. Ajilore[1]

Abstract

This study investigates non-slip hydromagnetic laminar dissipation flow with Arrhenius kinetics in binary reactions characterized by reaction order and variable properties within an unbounded isothermal device. The partial differentiation model is nondimensionalized to a thermofluidic dimensionless form. An invariant quasi-linear coupled ordinary derivative model is obtained using similarity quantities and solved using the Shooting scheme coupled with the Runge-Kutta method. Results show that species mixture reduces flow velocity but increases binary species reaction by 0.734%. Activation energy and material coefficients enhance the thermal profile within the flow medium. This provides insights for industrial development in selecting working fluid properties.

1. Introduction and Preliminaries

The flow of current-carrying fluid materials stimulated by magnetic force is presently given much attention owing to its usage in MHD generators, heat conductors, oil exploration, fusion and fission reactions, plasma, and so on, [1].

Received: 30/03/2006, Accepted: 05/05/2026, Revised: 08/06/2006. * Corresponding author.
2015 *Mathematics Subject Classification.* 37N10 & 76N17.
Keywords and phrases. No-slip condition; Activation energy; Reaction order; Arrhenius kinetics; Viscous dissipation.
[1]Department of Mathematical Sciences, Lagos State University of Science and Technology, Ikorodu, Nigeria
[2]Department of Mechanical Engineering, Lagos State University of Science and Technology, Ikorodu, Nigeria
E-mail of the corresponding author: raskareem4@yahoo.com
ORCID of the corresponding author: https://orcid.org/0000-0002-5733-6950

The magnetic-induced flowing fluid was reported to have supported the efficiency of industrial lubricant viscosity due to the impact of electromagnetic force that damped free flow and its ability to conduct heat away from a system, [7] and [20]. Several extensive researches have been performed on different magnetohydromagnetic fluid flow models in various geometries. Thus, [10] examined the dual solution of magneto-nanomaterial on a curved surface. The flow rate was reported to have been damped with rising magnetic terms.

[3] considered the thermo-physical impact of magnetic force on a nanofluid flow past a Couette horizontal device. It was found that magnetic force retarded the flow near the fixed surface. [16] examined considered magnetic viscous flow in a vertical configuration and reported that material properties supported the magnetic force in opposing the flow and increased fluid viscosity. [21] and [11] reported that a fluid material's viscosity property is sensitive to temperature changes.

Meanwhile, many industrial and technological processes for reacting species involving hydromagnetic flow are often accompanied by heat transfer, [22]. As such, [19] examined nanofluid exothermic species reaction in the porous cavity with a sloping magnetic field and heat transfer. It was presented that heat transfer is enhanced with a rising exothermic reaction, which reduces fluid viscosity. [9] theoretically examined the Maxwell mixed convective flow in an isothermal infinite stretchable disk with heat generation/sink. The findings show that the heat generation enhanced heat propagation and chemical reaction. In a vertical device, [15] examined the heat transport of chemically reacting hydromagnetic nanomaterial in a Maxwell base fluid with a heat sink. The magnetic field is seen to have increased heat transfer but damped the reacting fluid flow velocity. In practical phenomena, differences in the species concentration mixture led to mass transfer, which is useful in many industrial and chemical mixtures [23] and [26]. Every reacting species requires a minimum energy to stimulate the reaction.

The mechanism for reacting species of mass diffusion influenced by Arrhenius activation energy is often encountered in oil and water emulsions, food processing, chemical engineering, thermal reservoirs, and so on. No matter how small, fluid molecular reaction requires potential and kinetic energies for the Arrhenius chemical mixture, but as a result of pronounced momentum energy, small activation energy may be needed to break the molecular bond, [27]. The significance of the activation energy concept can be found in geothermal processes, oil industries, hydromagnetic processes, oil suspension, and others. Owing to its usefulness, [2] presented a binary chemical mixture and reduction of entropy generation in Arrhenius activation energy of radiative hydromagnetic nanomaterial flow past a vertical plate. It was stated that temperature field and thermal diffusion are enhanced with rising radiation variables. [4] investigated the nanofluid covalent bonding of cross-radiation in an axisymmetric flow with the Arrhenius activation

energy effect. The numerical outcomes depicted that the chemical concentration profile is raised with high activation energy. [14] investigated the influence of activation energy and buoyancy force on hydromagnetic chemically reacting nanofluid flow in a vertical medium. The numerical study shows that nanofluid concentration rises proportional to the Arrhenius chemical reaction rate. [24] the authors presented the entropy generation of an Oldroyd 8-constant hydromagnetic fluid in a double Arrhenius reaction and current density. From the analytical results, it was stated that the second exothermic reaction term enhances reaction combustion. Other investigations on the Arrhenius activation energy for different fluid materials can be found in [5, 6], [8] and [25].
This study focuses on the influence of varying heat generation, heat dissipation, and activation energy on a hydromagnetic heat transfer and chemical reaction occurring in an isothermal vertical device. The study is significant in chemical sciences, industrial processes, engineering and so on. Of many related studies or models, no combined effect of magnetic field, activation energy, varying heat source, and thermal dissipation have been examined despite their significance in many aspects of sciences and engineering. Hence, the usefulness of this study to the thermal chemical sciences motivated the interest. As such, the investigation is inspired by the phenomenal applications of the study coupled with the significant reports from various researchers as seen in [4], [6], [12] and [26]. A numerical analysis of the model is carried out using a shooting method combined with the Runge-Kutta scheme; the outcomes are given in the tables, graphs and qualitatively discussed.

2. Boundary Layer Flow Dimensional Model

A theoretical non-slip hydromagnetic laminar flow of chemical reacting fluid in a vertical boundless device is considered. The flow is influenced by viscous dissipation, varying heat sources, pressure gradient, and temperature-dependent thermal conductivity without reacting material species consumption. The fluid particles collided continuously without deformation, satisfying Newton's law of flow motion. The fluid chemical reaction is stimulated by branched reaction order, activation energy, internal heating, and chemical kinetics. The magnetic field controls the fluid conductivity strength at low Reynolds numbers with negligible magnetic induction. The boundary layer flow equations are formulated based on the highlighted assumptions, which follow from the recent works of [17] and [18]. Hence, the governing equations for velocity, energy, and mass transfer are formulated as:

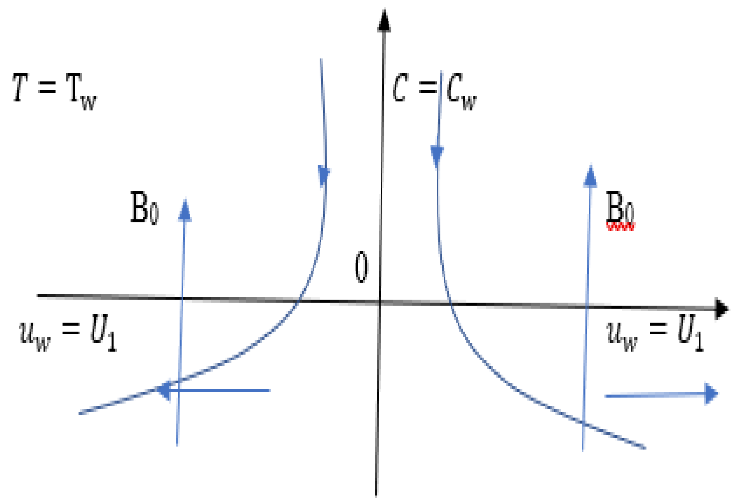

Figure 1: Physical flow configuration

(1)
$$u\frac{\partial u}{\partial x}+v\frac{\partial u}{\partial y}=-\frac{1}{\rho}\frac{\partial p}{\partial x}+\nu\left(\frac{\partial^2 u}{\partial x^2}+\frac{\partial^2 u}{\partial y^2}\right)-\frac{\sigma B^2}{\rho}(u-U)+g\beta_\tau(T-T_\infty)+\beta_c(C-C_\infty),$$
(2)
$$u\frac{\partial v}{\partial x}+v\frac{\partial v}{\partial y}=-\frac{1}{\rho}\frac{\partial p}{\partial y}+\nu\left(\frac{\partial^2 v}{\partial x^2}+\frac{\partial^2 v}{\partial y^2}\right)-\frac{\sigma B^2}{\rho}v,$$
(3)
$$\rho c_p\left(u\frac{\partial T}{\partial x}+v\frac{\partial T}{\partial y}\right)=\frac{\partial}{\partial y}\left(k_T\frac{\partial T}{\partial y}\right)+\mu\left(\frac{\partial u}{\partial y}\right)^2,$$
(4)
$$\rho\left(u\frac{\partial C}{\partial x}+v\frac{\partial C}{\partial y}\right)=D\frac{\partial^2 C}{\partial y^2}+\gamma(C-C_\infty)-k_r(T-T_\infty)^r\exp\left(-\frac{E_a}{R_G T}\right)(C-C_\infty).$$

With boundary conditions:

$$u=U_1,\ v=v_w,\ T=T_w,\ C=C_w\quad \text{at } y=0,$$

(5) $$u\to U,\ T\to T_\infty,\ C\to C_\infty\quad \text{as } y\to\infty.$$

The following appropriate variables are applied to the system of flow dimensional equations to obtain dimensionless transformed equations as demonstrated by [4] and [6].

$$
\begin{aligned}
&x' = \frac{x}{L}, \quad y' = \frac{y}{\delta}, \quad u' = \frac{u}{U}, \quad v' = \frac{v}{U}\frac{L}{\delta}, \quad p' = \frac{p}{\rho U^2}, \quad U' = \frac{U}{U_0},\\
&\omega' = \frac{4\nu\omega}{v_0^2}, \quad V = \frac{U_1}{U_0}, \quad (T - T_\infty) = \left(\frac{E_a}{R_G T_\infty^2}\right)^{-1}\theta(x,y),\\
&(C - C_\infty) = (C_w - C_\infty)\theta(x,y)
\end{aligned}
\tag{6}
$$

where L is scale length, δ is the unknown thickness of the device layer for which $x = L$, and U is the velocity of the flowing liquid along the x-axis parallel to the bounded flow medium layer.

Using these defined quantities, the non-dimensional flow system of equations (limit $R \to \infty$) becomes:

$$
\frac{\partial u}{\partial x} + \frac{\partial v}{\partial y} = 0 \tag{7}
$$

$$
u\frac{\partial u}{\partial x} + v\frac{\partial u}{\partial y} = G(x) + \frac{\partial^2 u}{\partial y^2} - H(u-1) \mp Fs(u-1) + Gr(N\theta + \phi) \tag{8}
$$

$$
u\frac{\partial \theta}{\partial x} + v\frac{\partial \theta}{\partial y} = \tau\frac{\partial}{\partial y}\left((1+\epsilon\theta)\frac{\partial \theta}{\partial y}\right) + \beta\left(\frac{\partial u}{\partial y}\right)^2 - \alpha_0\left[\alpha_1(u-1) + \theta\right] \tag{9}
$$

$$
u\frac{\partial \phi}{\partial x} + v\frac{\partial \phi}{\partial y} = \frac{1}{Sc}\frac{\partial^2 \phi}{\partial y^2} + \chi\phi - \epsilon\lambda\theta^r \exp\left(\frac{\theta}{1+\epsilon\theta}\right)\phi \tag{10}
$$

With boundary conditions:

$$
\begin{cases}
u = V,\ v = 0,\ \theta(x,0) = 1,\ \phi(x,0) = 1, & y = 0\\
u \to 1,\ \theta(x,y) \to 0,\ \phi(x,y) \to 1, & y \to \infty
\end{cases}
\tag{11}
$$

Thermo-fluid physical terms are respectively described as follows:

(12)
$$\frac{\sigma\mu B^2(x)L}{kU} = H, \quad \frac{g\beta_c(C_w - C_\infty)L}{U^2} = Gr, \quad \frac{\beta_\tau R_G T_\infty^2 L}{\beta_c E_a(C_w - C_\infty)U^2} = N,$$
$$g\frac{K_1}{\nu}\frac{L}{U}|\hat{u}| = Fs, \quad \frac{k}{\mu c_p}\frac{L}{U\delta^2 T_\infty} = \tau, \quad \frac{R_G T_\infty}{E_a} = \epsilon,$$
$$\frac{U^3\rho L}{\delta^2}\frac{E_a}{R_G T_\infty^2} = \beta, \quad \frac{2x\gamma L}{\rho U^2} = \chi,$$
$$\frac{A^*(T_w - T_\infty)E_a U}{B^* bx R_G T_\infty^2} = \alpha_1, \quad \frac{LB^*}{U}\frac{\kappa u_w(x)}{x\nu} = \alpha_0,$$
$$\frac{k_r^2 2xL}{\rho U^2}(\epsilon T_\infty)^r \exp\left(-\frac{1}{\epsilon}\right) = \lambda, \quad \frac{DL}{\mu U} = \frac{1}{Sc}, \quad R = \frac{UL}{\nu},$$
$$\frac{E_a}{R_G T_\infty^2} = \frac{\rho U^2}{\delta^2}\frac{1}{\epsilon T_\infty}$$

For the flow velocity U parallel to the flat vertical plate, the pressure is independent of y. The condition required at the controlling edge, an indefinite speed gradient $x = y = 0$, depicts that a mathematical singularity solution exists. Meanwhile, an approximate boundary layer implicit is assumed for drag fluid flow motion at the region along the leading edge. The solution given by the boundary layer approximation is not valid at the leading edge, but valid near the point $x = 0$. As such, the boundary layer equations (7)-(11) are reduced to single-variable independent equations for which the boundary value problem admits a similar solution.

A one-parameter variable transformation of y, x and ψ for which the dimensionless equations are invariant for ψ is described as:

(9)
$$\psi = \sqrt{2\nu U x}\, f(\eta), \quad v(x,y) = -\frac{\partial\psi}{\partial x} = \sqrt{\frac{U\nu}{2x}}\left(\eta f'(\eta) - f(\eta)\right),$$

(10)
$$\eta = \sqrt{\frac{U}{2\nu x}}\, y, \quad u = \frac{\partial\psi}{\partial y}, \quad v = -\frac{\partial\psi}{\partial x}, \quad u(x,y) = \frac{\partial\psi}{\partial y} = Uf'(\eta),$$

(13)
$$\eta_x = -\frac{1}{2x}\eta, \quad \eta_y = \sqrt{\frac{U}{2\nu x}}.$$

Using equation (9) on the dimensionless model, equation (7) is identically satisfied. Hence, equations (8)-(11) are transformed to become:

$$f'''(\eta)+f''(\eta)f(\eta)-(H\pm Fs)(f'(\eta)-1)+Gr(N\theta+\phi)+G=0 \tag{14}$$

$$\tau\left((1+\epsilon\theta(\eta))\theta'(\eta)\right)'+f(\eta)\theta'(\eta)+\beta\left(f''(\eta)\right)^2-\alpha_0\left[\alpha_1(f'(\eta)-1)+\theta(\eta)\right]=0 \tag{15}$$

$$\frac{1}{Sc}\phi''+f(\eta)\phi'+\chi\phi-\lambda\theta^r\exp\left(\frac{\theta}{1+\epsilon\theta}\right)\phi=0 \tag{16}$$

With boundary conditions:

$$\begin{cases} f'(\eta)=V,\ f(\eta)=0,\ \phi(\eta)=1,\ \theta(\eta)=1, & \eta=0\\ f'(\eta)\to 1,\ \phi(\eta)\to 0,\ \theta(\eta)\to 0, & \eta\to\infty \end{cases} \tag{17}$$

A reduced two-point boundary layer equation is obtained in the form:

$$f'''(\eta)+f''(\eta)f(\eta)=0 \tag{18}$$

Numerically, $f''(0)=0.469599988500248\approx 0.46960$ is obtained and the point solutions are presented in Figure 2.

The critical quantities of technological practices and applications are the wall friction, heat gradient, and concentration gradient; these are individually defined in dimensionless form as:

$$\tau=\left.\frac{du(\eta)}{d\eta}\right|_{\eta=0},\quad Nu=-\left.\frac{d\theta(\eta)}{d\eta}\right|_{\eta=0},\quad Sh=-\left.\frac{d\phi(\eta)}{d\eta}\right|_{\eta=0}. \tag{19}$$

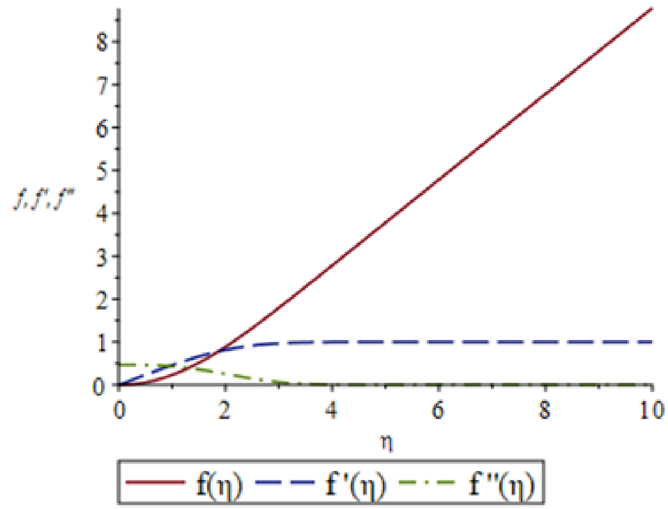

Figure 2: A one-parameter functions $f(\eta)$, $f'(\eta)$ and $f''(\eta)$.

The range of values at the horizontal axis denotes the range of values of η, while the vertical axis represents the functions $f(\eta)$, $f'(\eta)$ and $f''(\eta)$. The numerical point solutions for the flow field, velocity field, and wall velocity gradient are demonstrated in the plot.

2.1. **Numerical Computation Technique.** Now, to compute the numerical solution to the problem considered here. The solutions to the system of quasi-linear equations are solved for at the infinite regime $0 < \eta < \eta_\infty$. The solution technique is employed because of its consistency, convergence, and accuracy.

For physical interpretation of results, a finite regime along the η-direction is chosen. To ensure that the asymptotic conditions are not affected by an imposed finite domain, η is taken to be sufficiently large. An independent grid study demonstrates that the numerical domain $0 < \eta < \eta_\infty$ can be divided into a regular step size interval of 0.02. Thus, the number of points in the interval $0 < \eta < \eta_\infty$ is reduced with reasonable accuracy. Taking $\eta_\infty = 5$, this is found to be sufficient for the parameter range of values used in this study.

The heat and mass boundary layer governing equations and the corresponding boundary conditions were numerically solved. The mathematical software **Maple 2020** was used to run the code for numerical computation of the system of equations (10)-(14) along with initial and boundary conditions (17).

The numerical values of the flow governing parameters are chosen as:

$$\epsilon = N = \lambda = G = 0.1, \quad Pr = 7.0, \quad Sc = 0.6, \quad V = Fs = H = 0.2, \quad \beta = 0.04,$$

$$Gr = 0.5, \quad \delta = 0.05, \quad \alpha_0 = 0.02, \quad \alpha_1 = 0.05, \quad r = 1.0$$

based on existing related theoretical works.

3. Results and Discussion

In Table 1, the results of the present study are compared with previous ones and found to be in good agreement.

The computational outcomes for the fluid wall friction $f''(0)$, temperature wall gradient $\theta'(0)$ and wall mass transfer gradient $\phi'(0)$ are depicted in Table 2.

The engineering quantities' corresponding increase or decrease are observed as various parameter values are enhanced.

The tables show the sensitivity of the chemical reacting fluid and temperature to parameter variation. As such, these parameters should be monitored for effective usage of working fluids to enhance performance.

Table 1. Results verification with existing related studies

Terms		[13]		[17]		Present outcomes	
Pr	Sc	τ	Nu	τ	Nu	τ	Nu
0.50	0.71	3.09046	1.21628	3.09048	1.21627	3.09035	1.21657
0.70	0.71	2.77995	1.21263	2.77998	1.21262	2.78003	1.21239
0.60	1.00	2.79576	1.49400	2.79577	1.49399	2.79568	1.49410
0.60	5.00	1.75935	4.36421	1.75937	4.36421	1.75948	4.36457

TABLE 2. Effect of α_0, χ, G, H, N, and Gr on skin friction, temperature, and mass gradient

α_0	χ	G	H	N	Gr	$f''(0)$	$-\phi'(0)$	$-\theta'(0)$
0						1.1285264	-0.5077929	-0.5139627
0.2						1.1265668	-0.5072815	-0.6078117
0.4						1.1249422	-0.5068625	-0.6910885
1.0						1.1213691	-0.5059558	-0.8990935
	0.0					1.0626547	-0.8994555	-0.5172553
	0.5					1.0886094	-0.7319737	-0.5198783
	1.0					1.2623458	0.1043590	-0.5372888
	3.0					1.7512308	2.0775658	-0.5768939
		0.0				0.9799411	-0.4876214	-0.5075284
		0.5				1.6910721	-0.5724704	-0.5720068
		1.0				2.3456045	-0.6329471	-0.6082391
		3.0				4.6745359	-0.7876058	-0.6375864
			0.0			1.0774817	-0.5066292	-0.5229433
			0.4			1.1784640	-0.5089507	-0.5249500
			1.2			1.3684251	-0.5140091	-0.5290248
			2.0			1.5404663	-0.5186606	-0.5325403
				0.0		1.0947979	-0.5050664	-0.5217401
				0.5		1.2598287	-0.5179152	-0.5320689
				1.0		1.4191753	-0.5296643	-0.5411629
				1.5		1.5737389	-0.5405211	-0.5492400
					0.0	0.7287420	-0.4724569	-0.4940437
					1.0	1.4913757	-0.5355235	-0.5455688
					3.0	2.7548605	-0.6132785	-0.5935911
					5.0	3.8569849	-0.6668174	-0.6115227

The flow velocity dimension sensitivity to a rising pressure gradient (G), Hartmann number (H), and Grashof number (Gr) are respectively offered in Figures 3, 4, and 5. As seen in Figure 3, the change rate of the term G with respect to the distance η increases the velocity profile. The pressure gradient exerts a force normal to the directional isobaric surface, balancing gravitational force and enhancing liquid particle collisions along the stream. Hence, the pressure gradient boosts the magnitude of the flow rate.

In Figure 4, the Hartmann number stimulates electromagnetic force (Lorentz force), dragging the velocity distribution near the bounded plate. The flow velocity is propelled along the stream due to rising heat generation. The electromagnetic force dominates the viscous fluid, thereby reducing the conducting fluid velocity profile past a magnetic field near the plate.

Figure 5 shows that the rising Grashof number encourages the velocity profile. The buoyancy force ratio dominates the viscous force, stimulating natural convection and leading to a significant rise in flow rate magnitude. A rise in temperature change reduces fluid density variations, enhancing the velocity field.
Figure 6 demonstrates the chemical reaction effect (χ) on species transfer. A noteworthy rise in mass transfer is observed due to reduced viscosity and increased heat source formulated by reaction kinetics and activation energy. Heat dispersion propels the chemical reaction rate, encouraging molecular interaction and enhancing flow rate and concentration distribution.
Figures 7 and 8 show that the limiting velocity (V) and buoyancy ratio (N) increase the laminar Newtonian flow velocity profile. A continuous rise in velocity along the bounded stream is observed due to the dominance of heat generation over fluid viscosity. The molecular bond is reduced, enhancing fluid mixture and raising flow dimension. This aligns with existing reports in the literature [3, 17].
Figures 9 and 10 illustrate the impact of the binary reacting mixture term (λ) on velocity and concentration diffusion. Flow characteristics decrease with rising binary reaction parameters because bimolecular kinetics are damped and electromagnetic force is enhanced. As a result, molecular bonding restricts open collisions of liquid elements, reducing both velocity profile and mass transport field.

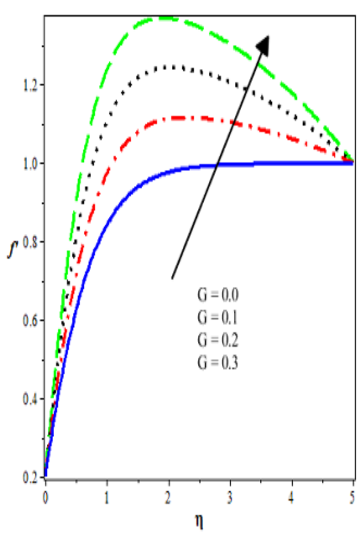

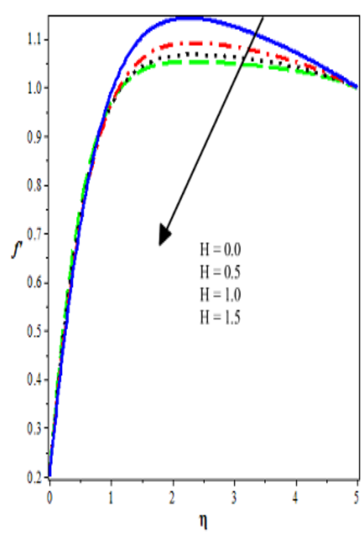

Figure 3: Velocity field for values of (G)
Figure 4: Heat field for various values of (H)

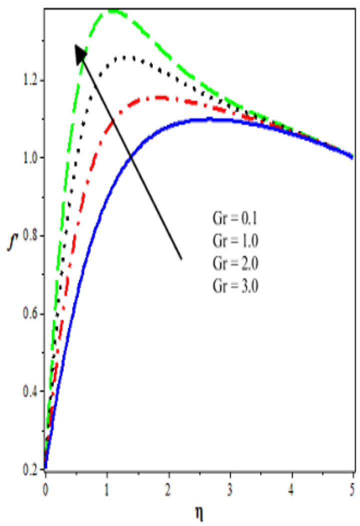

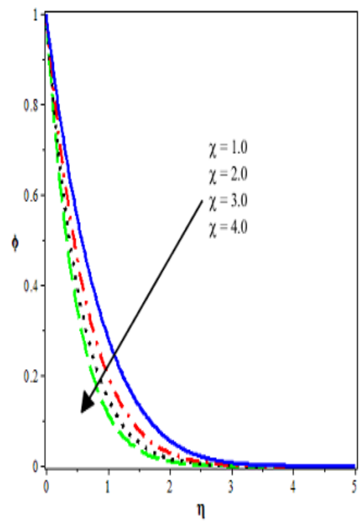

Figure 5: Impact of Grashof number (Gr) on flow rate profile
Figure 6: Velocity distribution for rising chemical reaction parameter (χ)

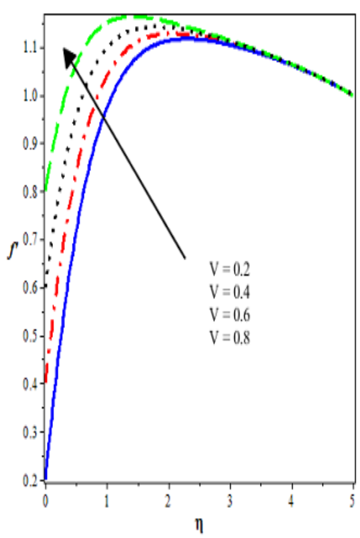

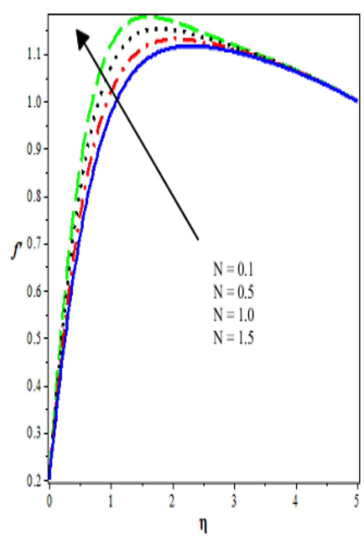

Figure 7: Flow rate profile for rising limiting velocity (V)
Figure 8: Velocity field for various buoyancy ratio (N)

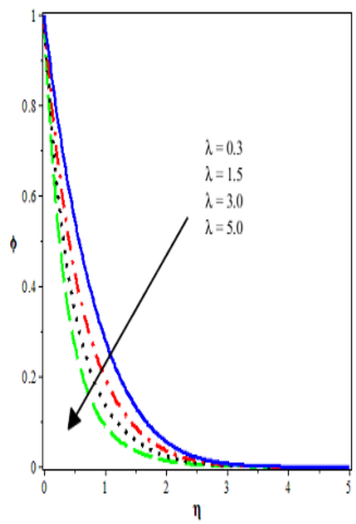

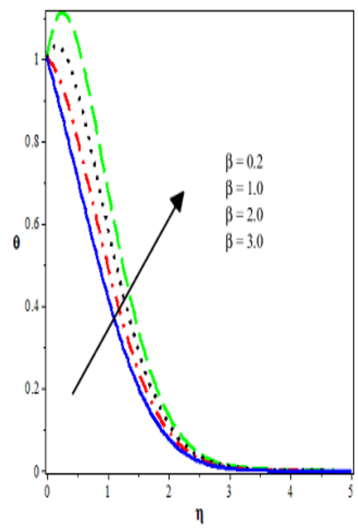

Figure 9: Effect of binary reacting mixture term (λ) on velocity profile
Figure 10: Mass profile field for various binary reacting mixture term (λ)

Conclusion. A numerical investigation of the continuous non-slip flow of hydromagnetic Arrhenius kinetics fluid reaction with thermal conductivity and heat generation variable properties is carried out in a vertical medium. The flow characteristics of the thermo-fluid entrenched parameters and the reactive species diffusion rate sensitivity are established numerically. The behaviour of the Arrhenius reactive kinetics fluid along the bounded plate surface is presented in tables for various fluid physical terms.

The observations from the study are summarized as follows:

- Enhancing the values of V, Gr, β, and χ causes a monotonic rise in the function η for the respective flow velocity, thermal diffusion and mass transfer.
- The Arrhenius kinetics supports the activation energy to increase the species heat conductivity of the temperature field.
- The combined effect of activation energy and chemical kinetics stimulates the terms G and N, significantly increasing the flow velocity.
- Fluid viscosity is augmented with rising parameters H and λ by conducting heat away from the reactive fluid material.

This study will assist lubricant oil production, synthetic chemical manufacturing, and related industries in improving their working fluid for enhanced productivity. Furthermore, the study can be extended to viscoelastic fluid materials flow in concentric or annular cylinders.

Acknowledgement: The authors are grateful to Lagos State University of Science and Technology, Nigeria for the supports they received during the compilation of this work.

Competing interests: The manuscript was read and approved by all the authors. They therefore declare that there is no conflicts of interest.

Funding: The Authors received no financial support for the research, authorship, and/or publication of this article.

References

[1] Acharya N. (2021). Spectral quasi linearization simulation on the radiative nanofluid spraying over a permeable inclined spinning disk considering the existence heat source/sink. *Applied Mathematics and Computation*. **411**, 166-173. 126547.

[2] Acharya N., Maity S. & Kundu P. K. (2020). Differential transformed approach of unsteady chemically reactive nanofluid flow over a bidirectional stretched surface in the presence of magnetic field. *Heat Transfer*. **49**, 3917-3942.

[3] Ahmed Z., Al-Qahtani A., Nadeem S. & Saleem S. (2019). Computational study of MHD nanofluid flow possessing micro-rotational inertia over a curved surface with variable thermo-physical properties. *Processes*. **7**, 387-394.

[4] Azama M., Xu T., Shakoor A. & Khan M. (2022). Effects of Arrhenius activation energy in development of covalent bonding in axisymmetric flow of radiative-Cross nanofluid. *International Communications in Heat and Mass Transfer*. **113**, 56-64. 104547.

[5] Dawar A. & Acharya N. (2022). Unsteady mixed convective radiative nanofluid flow in the stagnation point region of a revolving sphere considering the influence of nanoparticles diameter and nanolayer. *Journal of the Indian Chemical Society*. **99**, 109-116. 100716.

[6] Dhlamini M., Mondal H., Sibanda P. & Motsa S. (2020). Activation energy and entropy generation in viscous nanofluid with higher order chemically reacting species. *International Journal of Ambient Energy*. **14**, 1-13.

[7] Fatunmbi E. O. & Okoya S. S. (2020). Heat transfer in boundary layer magneto-micropolar fluids with temperature-dependent material properties over a stretching sheet. *Advances in Materials Science and Engineering*. **20**, 1-11.

[8] Hayat T., Ullah I., Waqas M. & Alsaedi A. (2019). Attributes of activation energy and exponential based heat source in flow of Carreau fluid with cross-diffusion effects. *Journal of Non-Equilibrium Thermodynamics*. **49**, 1-10.

[9] Khan N., Hossam A. N., Hashmi M. S., Khan S. U. & Tlili I. A. (2020). Theoretical analysis for mixed convection flow of Maxwell fluid between two infinite isothermal stretching disks with heat source/sink. *Symmetry*. **12**, 1-18.

[10] Khan A. U., Hussain S. T. & Nadeem S. (2019). Existence and stability of heat and fluid flow in the presence of nanoparticles along a curved surface by means of dual nature solution. *Applied Mathematics and Computation*. **353**, 66-81.

[11] Khan M. I., Qayyum S., Hayat T., Waqas M., Khan M. I. & Alsaedi A. (2023). Entropy generation minimization and binary chemical reaction with Arrhenius activation energy in MHD radiative flow of nanomaterial. *Journal of Molecular Liquids*. **259**, 274-283.

[12] Kumar G. K., Ramesh G. K., Gireesha B. I. & Rashad A. M. (2026). On stretched magnetic flow of Carreau nanofluid with slip effects and nonlinear thermal radiation. *Nonlinear Engineering*. **8**, 340-349.

[13] Makinde O. D. (2025). Free convection flows with thermal radiation and mass transfer past a moving vertical porous plate. *International Communications in Heat and Mass Transfer*. **32**, 1411-1419.

[14] Mustafa M., Khan J. A., Hayat T. & Alsaedi A. (2024). Buoyancy effects on the MHD nanofluid flow past a vertical surface with chemical reaction and activation energy. *International Journal of Heat and Mass Transfer*. **108**, 1340-1346.

[15] Nadeem S., Akhtar S. & Abbas N. (2020). Heat transfer of Maxwell base fluid flow of nanomaterial with MHD over a vertical moving surface. *Alexandria Engineering Journal*. **59**, 1847-1856.

[16] Nadeem S., Khan M. R. & Khan A. U. (2019). MHD stagnation point flow of viscous nanofluid over a curved surface. *Physica Scripta*. **94**, 456-463. 115207.

[17] Okedoye A. M., Salawu S. O., & Asibor E. A. (2021). A convective MHD double diffusive flow of a binary mixture through an isothermal and porous moving plate with activation energy. *Computational Thermal Sciences*. **13**, 45-60.

[18] Olanrewaju A. M., Salawu S. O., Olanrewaju P. O. & Amoo S. A. (2021). Unsteady radiative MHD flow and entropy generation of Maxwell nanofluid in porous media with Arrhenius chemical kinetic. *Cogent Engineering*. **8**, 222-234. 1942639.

[19] Rahman M. M., Pop I., & Saghir M. Z. (2019). Steady free convection flow within a tilted nanofluid saturated porous cavity in the presence of a sloping magnetic field energized by an exothermic chemical reaction administered by Arrhenius kinetics. *International Journal of Heat and Mass Transfer*. **129**, 198-211.

[20] Reddy M. G., Kumar N., Prasannakumara B. C., Rudraswamy N. G. & Kumar K. G. (2021). Magnetohydrodynamic flow and heat transfer of a hybrid nanofluid over a rotating disk by considering Arrhenius energy. *Communications in Theoretical Physics*. **73**, 79-88. 45002.

[21] Rehman F., Khan M. I., Sadiq M. & Malook A. (2017). MHD flow of carbon in micropolar nanofluid with convective heat transfer in the rotating frame. *Journal of Molecular Liquids*. **231**, 353-363.

[22] Salawu S. O. & Dada M. S. (2018). Lie group analysis of Soret and Dufour effects on radiative inclined magnetic pressure-driven flow past a Darcy-Forchheimer medium. *Journal of the Serbian Society for Computational Mechanics*. **12**, 108-125.

[23] Salawu S. O., Disu A. B. & Dada M. S. (2020). On criticality for a generalized Couette flow of a branch-chain thermal reactive third-grade fluid with Reynolds viscosity model. *The Scientific World Journal*. **20**, 10 pages.

[24] Salawu S. O., Oderinu R. A. & Ohaegbue A. D. (2021). Current density and thermodynamic analysis of energy optimization for double exothermic reaction of magneto-Oldroyd 8-constant material. *Journal of King Saudi University - Science*. **33**, 10 pages. 101374.

[25] Salawu S. O. & Okoya S. S. (2021). On criticality for a branched-chain thermal reactive diffusion in a cylinder. *Combustion Science and Technology*. **192**, 1-16.

[26] Shamshuddin MD., Rajput G. R., Mishra S. R. & Salawu S. O. (2023): Radiative and exponentially space-based thermal generation effects on an inclined hydromagnetic aqueous nanofluid flow past thermal slippage saturated porous media. *Int. J. of Modern Physics* **B 23**, 611-623. 50202.

[27] Waqas H., Khan S. U., Shehzad S. A. & Imran M. (2019): Radiative flow of Maxwell nanofluid containing gyrotactic microorganism and energy activation with convective Nield conditions. *Heat Transfer Asian Research*. **48**, 1663-1687.

Nomenclature

K_T & Variable thermal conductivity
k & Uniform thermal conductivity
u, v & Velocities in x and y axes
C & Fluid chemical species
D & Species diffusion
R & Reynolds number
U & Velocity of the far stream
C_∞ & Concentration of the far stream
H & Hartmann number
T & Fluid temperature
c_p & Specific heat at constant pressure
E_a & Activation energy
R_G & Universal gas constant
g & Gravitational acceleration
r & Positive integer
Gr & Grashof number
N & Buoyancy ratio
Fs & Darcy Forchheimer parameter
V & Limiting velocity
Sc & Schmidt number
Pr & Prandtl number
θ & Dimensionless liquid temperature
ϕ & Dimensionless liquid chemical reaction
β & Material constants coefficient
γ & Reactivity parameter
λ & Binary chemical reaction parameter
ϵ & Positive number $(0 < \epsilon \ll 1)$